Revista Facultad de Ingeniería

Title: Interaction of supersonic discharge flow in parallel nozzles

Authors: Zain Ángel Mamaní[1] https://orcid.org/0009-0003-4551-8444 , Franco Picco[2] https://orcid.org/0009-0003-7960-8966 and Sergio Elaskar[2*] https://orcid.org/0000-0001-9718-7673

[1] División de Calidad de Mantenimiento Aeronáutico, Fábrica Argentina de Aviones – FAdeA-. Avenida Fuerza Aérea Argentina 5505. Córdoba, Argentina.

[2]Departamento de Ingeniería Aeroespacial, Instituto de Estudios Avanzados en Ingeniería y Tecnología -IDIT-, Universidad Nacional de Córdoba. Pabellón Argentina, Avenida Haya de la Torre s/n, Ciudad Universitaria X5000HUA. Córdoba, Argentina.

Corresponding Author: Sergio Elaskar
E-mail: selaskar@unc.edu.ar

DOI: **10.17533/udea.redin.20251087**

To appear in: *Revista Facultad de Ingeniería Universidad de Antioquia*

Received: October 22, 2024
Accepted: October 15, 2025
Available Online: October 15, 2025

Revista Facultad de Ingeniería, October, 2025

Interaction of supersonic discharge flow in parallel nozzles

Interacción del flujo supersónico de descarga en toberas en paralelo

Authors: Double-blind review

KEYWORDS:
OpenFOAM; gas dynamics equations; computer fluid dynamics

OpenFOAM; ecuaciones gasdinámicas; mecánica de fluidos computacional

ABSTRACT: This study focuses on the numerical analysis of the interaction between the exit flows of two supersonic nozzles, using the distance between their longitudinal axes as a parameter. The analysis is conducted in OpenFOAM, assuming two-dimensional, inviscid flow. The methodology employed to simulate flow in a nozzle is validated against experimental data and is subsequently used to investigate the interaction with a second nozzle. The numerical results indicate that discharge flows interfere, even from distant nozzles.

RESUMEN: Este estudio se centra en el análisis numérico de la interacción entre los flujos de salida de dos toberas Laval, utilizando como parámetro la distancia entre sus ejes longitudinales. El análisis se lleva a cabo con OpenFOAM bajo los supuestos de un flujo bidimensional y no viscoso. La metodología empleada en la simulación del flujo en una tobera se valida frente a datos experimentales y posteriormente se la utiliza para investigar la interacción con una segunda tobera. Los resultados indican que existe interferencia entre los flujos de descarga inclusive para toberas alejadas entre sí.

1. Introduction

The study of nozzles plays a crucial role in various engineering applications, including flow measurement, fuel injection, turbines, jet propulsion, etc. [1–7]. This work specifically focuses on jet propulsion. In fields such as rocketry and aviation, understanding the flow conditions at the nozzle's exit is essential, as it directly affects the intensity and direction of the thrust generated by the gases. Numerous investigations have been conducted on these topics.

The discharge flow from supersonic, axisymmetric nozzles into calm air was investigated to determine how the nozzle geometry and pressure ratio affect the exit flow. Through both theoretical and experimental methods, nozzles with various divergence angles, which resulted in a series of different Mach numbers at their exits, were examined. The analysis also included changing the static pressure ratio [8].

A numerical study on the exit flows of nozzles with different inlet geometries and pressure ratios ranging from 2 to 10 was conducted [9]. Additionally, numerical and experimental investigations were performed to assess the influence of nozzle geometry on supersonic exit flow, considering pressure ratios of up to 90 [10].

The phenomenon of thrust vectoring in supersonic nozzles, achieved through the injection of a secondary flow perpendicular to the main one, has been numerically studied as an alternative to classic mechanical methods [11].

On the other hand, the flow inside the nozzle has also been investigated. Specifically, numerical and experimental studies on how the flow separates from the wall in over-expanded nozzles have been conducted [12]. Additionally, the same phenomena were studied by solving the RANS equations numerically with a two-equation turbulence model k-ω [13].

Considering that many rockets feature multiple nozzle configurations, an additional factor must be addressed in the original problem. The discharge flow from one nozzle can disturb the exit flow of other nozzles, and vice versa. Therefore, the influence on the velocity and pressure fields at the exit of two parallel nozzles is studied as a function of the distance between their symmetry axes.

The solution to this problem cannot be determined analytically. Therefore, numerical simulations are performed using computational fluid dynamics (CFD) software. The numerical results are then compared with experimental data. The open-source code OpenFOAM [14] is employed through the *rhoCentralFoam* solver, as it has been implemented and validated by our research group to accurately describe supersonic flows, with and without chemical reactions [15–19].

This work is divided into five sections, starting with

this introduction. In Section 2, nozzles are briefly defined, and their governing equations are presented. The implemented methodology and its validation are in Section 3. In sections 4 and 5, the obtained numerical results are presented, and the main conclusions are drawn.

2. Theoretical Framework

2.1 Nozzles

A nozzle is a device that accelerates a flow at the expense of its pressure and temperature. The design of the nozzle depends on the desired flow velocities, as explained below. When analyzing the flow of compressible gases through a variable cross-section duct, certain simplifications can be applied. If the duct features a slight divergence and curvature and its diameter is small relative to the radius of curvature, it is possible to consider the transverse velocities to be negligible compared to the axial velocity. Additionally, both pressure and velocity can be treated as constant within each section of the duct. In summary, the quasi-one-dimensional flow hypothesis can be utilized, as the flow properties depend solely on the longitudinal coordinate and the cross-section, which varies as a function of the longitudinal position within the duct [20].

It can be demonstrated that under these conditions, the flow Mach number is related to the area of the cross section via Equation (1):

$$\left(\frac{A}{A^*}\right) = \frac{1}{M}\left[\frac{2}{\gamma+1}\left(1+\frac{\gamma+1}{2}M^2\right)\right]^{\frac{\gamma+1}{\gamma-1}} \quad (1)$$

In subsonic flows ($M < 1$), the cross-sectional area must decrease in the direction of flow to allow for an increase in the kinetic energy of the gas. Nozzles designed this way are called convergent nozzles. In contrast, when dealing with supersonic flows ($M > 1$), the duct area needs to expand to achieve a similar increase in kinetic energy, leading to what is known as a divergent nozzle.

A Laval nozzle incorporates both convergent and divergent sections. At the top of Figure 1, a convergent-divergent nozzle is depicted. This design is specifically used to achieve supersonic flow at its exit. This nozzle can exhibit different behaviors depending on the pressure ratio between the inlet and the exit. The bottom of Figure 1 shows the ratio of static to stagnation pressure as a function of the longitudinal position within the nozzle for various cases.

In case H, the stagnation pressure at the inlet is insufficient for the flow to reach sonic speeds at the throat, resulting in a subsonic flow throughout the entire nozzle, which means the maximum mass flow rate is not achieved. Curve G illustrates the borderline case where the pressure ratio is just enough to reach a Mach number of 1 (M=1) at the throat, but it does not allow for the development of supersonic flow in the divergent section.

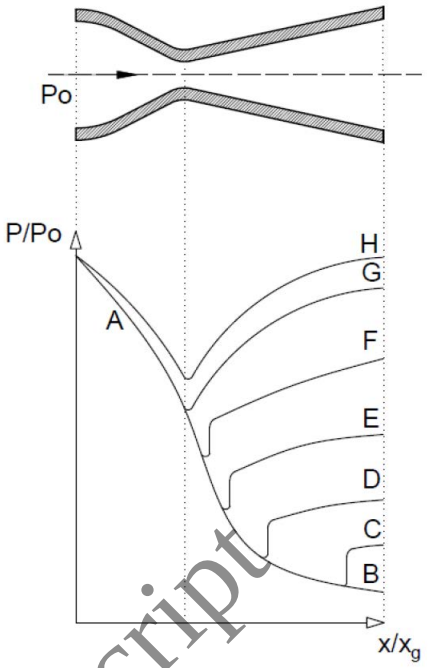

Figure 1 Static and stagnation pressure ratio as a function of longitudinal coordinate in a Laval nozzle.

In contrast, cases F, E, D, and C show that the flow continues to accelerate to supersonic speeds in the divergent section, although it does not possess enough energy to maintain supersonic speeds along its entire length. Consequently, a shockwave forms in the divergent section, with its position moving closer to the exit of the nozzle as the pressure ratio increases.

Lastly, curve B represents the ideal scenario where the flow remains supersonic throughout the entire length of the divergent section, with no shockwave forming. This last case, called the design condition, is considered optimum, as it enables supersonic discharge flows and maximizes mass flow rates.

The characteristics of the discharge flow beyond the nozzle exit depend on the ambient and exit pressure ratio. This flow is classified as under-expanded, optimally expanded, or over-expanded (see Figure 2). For an under-expanded nozzle, when the static pressure at the exit is higher than the atmospheric or ambient pressure, the discharge flow expands through an expansion fan. In Figure 3, it can be seen that the pressure in zone 1 is greater than the ambient pressure. Through the expansion fan, the flow pressure is equalized with atmospheric or ambient pressure in

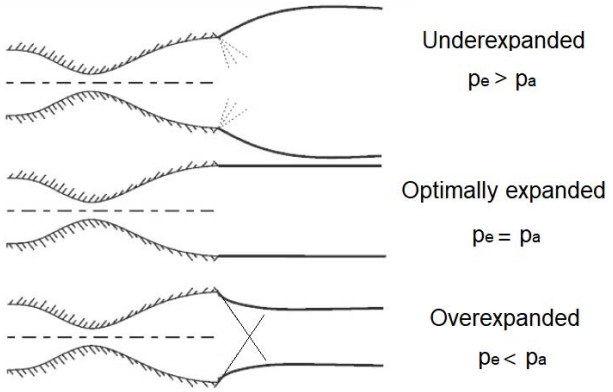

Figure 2 Discharge flow classification.

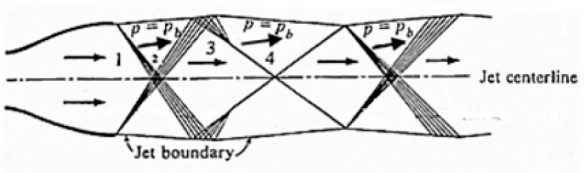

Figure 3 Under-expanded nozzle.

zone 2. However, the flow then encounters a second expansion fan, which is a reflection wave of the first one along the jet center line or symmetry line, causing the pressure to decrease again. Consequently, the pressure in zone 3 falls below ambient pressure, then rises to atmospheric pressure in zone 4 due to an oblique shock wave. In the following zone, another shock wave causes the pressure to increase again, and this repeating process continues until it is dissipated by viscous effects.

If the static pressure at the nozzle exit is lower than the ambient pressure, the nozzle is considered to be over-expanded. In this situation, a wave structure, as illustrated in Figure 4, forms and continues to repeat itself until it dissipates due to viscous effects.

The process begins with an oblique shock wave that increases the pressure of the discharged flow to match the ambient or atmospheric pressure. Subsequently, the flow encounters the reflection of this shock wave at the jet's center line, resulting in an additional increase in pressure. At this point, the pressure of the flow exceeds the ambient pressure. However, as the flow travels through an expansion fan and its reflection, the pressure again drops below atmospheric pressure. After this, the process starts anew.

If the exit and ambient pressures are equal, no expansion fans or shock waves appear, and the nozzle is considered to be optimally expanded.

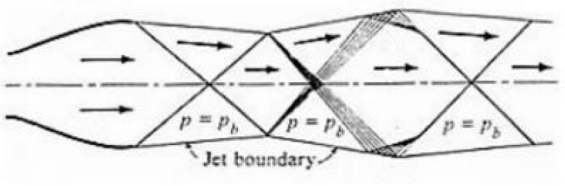

Figure 4 Over-expanded nozzle.

2.2 Governing equations

In this study, a compressible, two-dimensional flow is considered. This implies that the problem variables do not change in the direction perpendicular to the flow or that any changes in that direction are negligible. Additionally, the molecular transport phenomena are neglected, meaning that viscosity and thermal conductivity are not considered. With these assumptions, the equations for mass, momentum, and energy conservation are described, which lead to the Euler equations for gas dynamics. The resulting system of equations, as presented in [21], can be expressed as seen in Equations (2) through (5).

$$\frac{\partial}{\partial t}\int_{\Omega}\vec{W}d\Omega+\oint_{\partial\Omega}\vec{F}_{C}ds=\int_{\Omega}\vec{Q}d\Omega\,, \tag{2}$$

where $\vec{W}$ is the conservative variables vector

$$\vec{W}=\begin{bmatrix}\rho\\ \rho u\\ \rho v\\ \rho E\,.\end{bmatrix} \tag{3}$$

and $\vec{F}_C$ is the flux vector that contains the convective transport terms

$$\vec{F}_{C}=\begin{bmatrix}\rho uV\\ \rho uV+n_{x}p\\ \rho vV+n_{y}p\\ \rho HV\end{bmatrix} \tag{4}$$

The vector $\vec{Q}$ represents the contributions from volume forces and heat generation sources

$$\vec{Q}=\begin{bmatrix}0\\ \rho f_{e,x}\\ \rho f_{e,y}\\ \rho\vec{f_{e}}\cdot\vec{v}+\dot{q}_{h}\end{bmatrix} \tag{5}$$

In this last equation, ρf_e are the forces per unit of volume and $\dot{q}_h$ is the heat flow per unit of mass.

For two-dimensional flows, the Euler equations consist of four equations: mass conservation, momentum conservation in the x and y directions, and energy conservation. However, these equations involve five unknown variables: density (ρ), velocity in the x

direction (u), velocity in the y direction (v), total energy (E), and pressure (p). To fully describe the physical phenomenon, it is necessary to include thermodynamic equations that relate these state variables. In this context, the fluid is assumed to behave like a perfect gas, which means that density, pressure, and temperature are connected through Equation (6), also known as the equation of state [22].

$$p = \rho RT \tag{6}$$

For a perfect gas, the specific heats are constant, so the internal energy can be related to temperature [20].

3. Methodology

This section describes the numerical method, the validation analysis, and the meshes that have been implemented.

3.1 Finite volumes

Since the Euler equations do not have general analytical solutions, the finite volumes method is employed to discretize the original continuous domain into a set of control volumes. Within each control volume, the algebraic form of the transport equation is solved, resulting in a system of equations that can be solved numerically. As previously noted, the software used to solve this problem is OpenFOAM, and the specific solver implemented is *rhoCentralFoam* [14].

3.2 Validation

The geometry of the nozzle analyzed in this study is based on that used in a previous experimental work [12]. The dimensions of the nozzle and its domain, along with the corresponding boundary conditions, are illustrated in Figure 5. It is important to note that the experimental work only examines half of the nozzle, defined by its symmetry axis. In contrast, this investigation models the complete nozzle. The domain and boundary conditions for this case are presented in Figure 6.

Using Gmsh [23], six meshes were created with 48770, 54092, 67529, 110879, 116660, and 174021 elements, respectively. In each case, the mesh is refined in areas with high variable gradients, such as the walls and the nozzle exit. Conversely, the mesh is less dense in regions away from these areas.

Simulations were conducted using each of these meshes, taking into account the following initial conditions:

- $p_a = 102387.15 \ \ [Pa]$
- $p_0 = 555245.51 \ \ [Pa]$

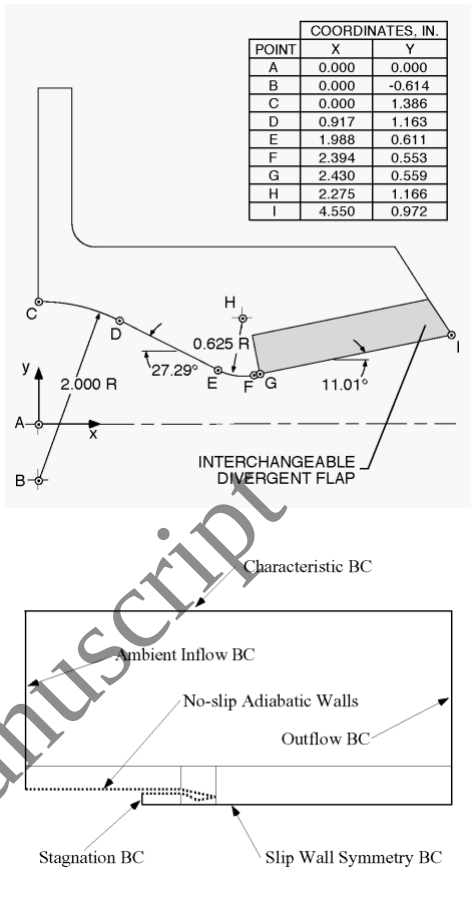

Figure 5 Laval nozzle used in the experimental study. (a) Geometry. (b) Domain.

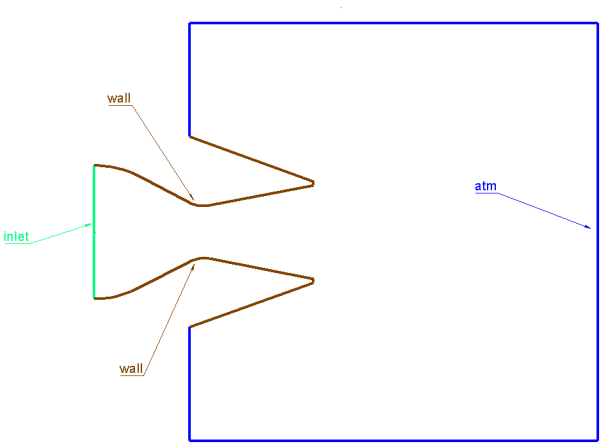

Figure 6 Complete Laval nozzle domain.

Table 1 Boundary conditions for a single Laval nozzle.

Contour	P [Pa]	T [K]	U [m/s]
inlet	555245.51	294.4	Computed
wall	zeroGradient	zeroGradient	slip
atm	zeroGradient	zeroGradient	zeroGradient

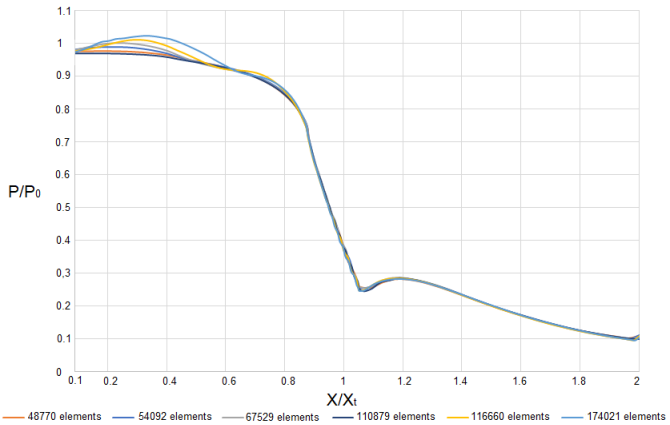

Figure 7 Comparison of the results obtained.

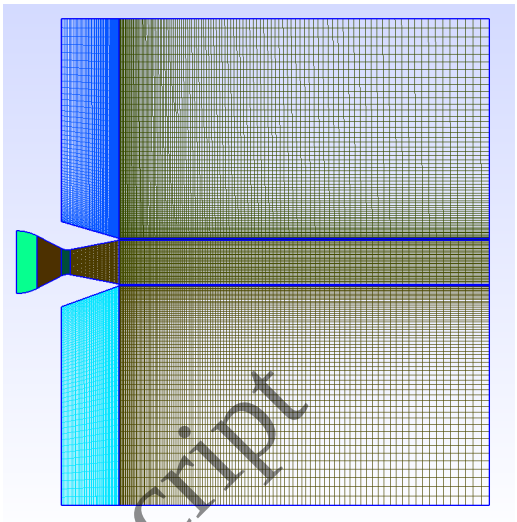

Figure 8 110879 elements mesh.

- $T = 294.4\ \ [K]$
- $U = 0\ \ [m/s]$

And the boundary conditions are specified in Table 1. In Figure 7, the simulation results for a stagnation to atmospheric pressure ratio of 5.423 are presented. The vertical axis displays the static and stagnation pressure ratio at the wall as a function of position along the nozzle.

The observed variations are small, particularly for the three denser meshes. This indicates that the solution is independent of element size. Notably, the results from the 110879 elements mesh align most closely with the experimental data used as reference [12]. Therefore, this mesh, displayed in Figure 8, is utilized to validate the methodology by comparing the numerical results with both experimental and theoretical data.

In Figure 9, the static and stagnation pressure ratio at the wall (vertical axis) is plotted as a function of the dimensionless position in the nozzle relative to the throat position (horizontal axis). The numerical results obtained are compared with experimental data and theoretical results. The figure illustrates that the simulation results align well with the experimental data. Additionally, they resemble previous results presented by other authors [24], indicating that the physical and numerical models used are appropriate. It is important to note that the theoretical model depicted in the figure corresponds to one-dimensional flow analysis [20].

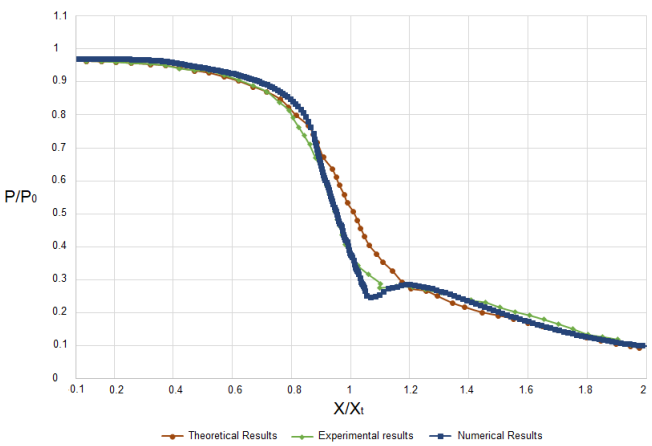

Figure 9 Pressure ratios at the nozzle wall.

Table 2 Boundary conditions for two parallel Laval nozzles.

Contour	P [Pa]	T [K]	U [m/s]
Inlet1	555245.51	294.4	Computed
Inlet2	555245.51	294.4	Computed
wall1	zeroGradient	zeroGradient	slip
wall2	zeroGradient	zeroGradient	slip
wall3	zeroGradient	zeroGradient	slip
wall4	zeroGradient	zeroGradient	slip
wall	zeroGradient	zeroGradient	slip
atm	zeroGradient	zeroGradient	zeroGradient

3.3 Parallel nozzles

The interaction between the discharge flows of two parallel nozzles is studied. Therefore, a parametric study with the separation between the two nozzles is carried out. The following distances between longitudinal axes are considered in this analysis:

- Case 1. 70.4 mm. Number of elements: 164392
- Case 2. 105.6 mm. Number of elements: 174085
- Case 3. 140.8 mm. Number of elements: 183145
- Case 4. 281.6 mm. Number of elements: 188635
- Case 5. 422.4 mm. Number of elements: 199495
- Case 6. 563.2 mm. Number of elements: 221215
- Case 7. 846.8 mm. Number of elements: 221215

Figure 10 shows the domains for cases with separations of 140.8 mm and 563.2 mm.
Due to CPU time constraints, Cases 6 and 7 share the same number of mesh elements, despite differing physical domain sizes. The physical domain for the last case is higher than that for Case 6. Therefore, in Case 7, the size of the elements was increased in areas where the gradients of the flow variables are null or small.
The initial conditions are the same as those stated previously, and the boundary conditions are illustrated in Figure 11 and listed in Table 2.

4. Results

Numerical results calculated at a time $t = 0.008$ s, from which the phenomenon is stationary, are shown. For all tests, the flow discharges to atmospheric conditions. In Figures 12 to 18 the velocity and pressure fields for each case can be seen. Figure 19 shows the pressure fields for the 105.6 mm and 140.8 mm cases, in this image the scale has been changed to better appreciate

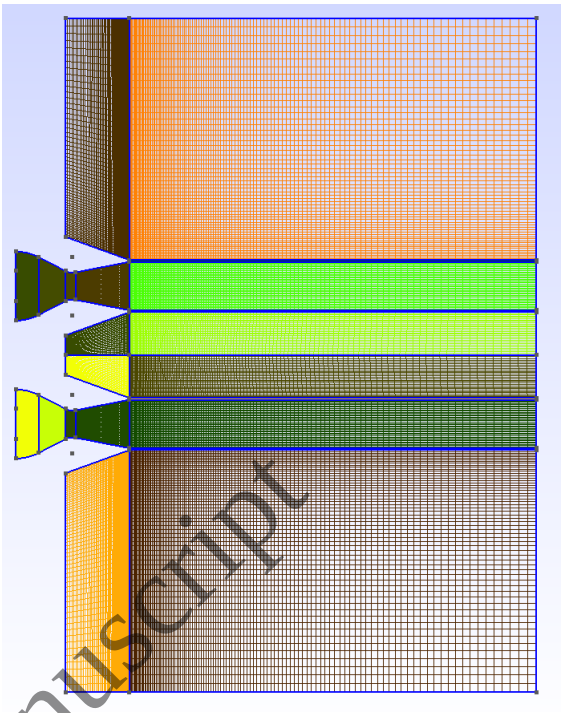

(a) Separation: 140.8 mm. 183145 elements.

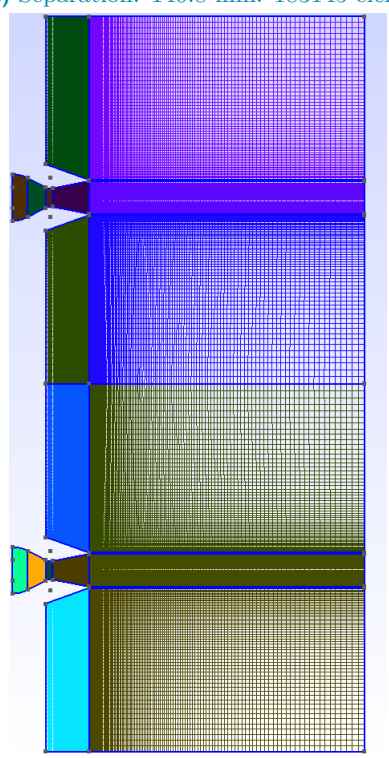

(b) Separation: 563.2 mm. 221215 elements.

Figure 10 Domain discretizations for two of the study cases.

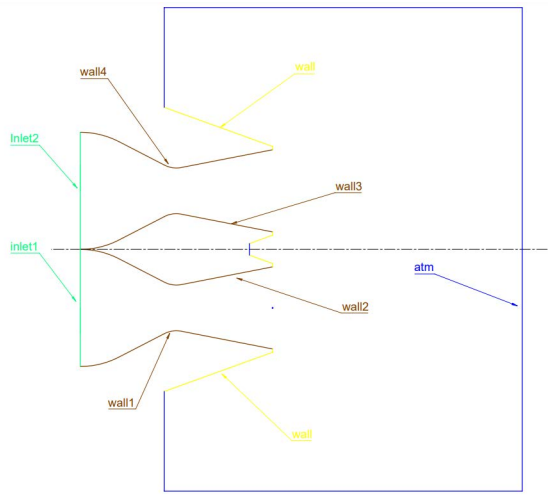

Figure 11 Geometry and boundary conditions.

the interaction between the jets. On the other hand, Figure 20 shows the static and atmospheric pressure ratio along the longitudinal axes of the nozzles for the 70.4 mm, 140.8 mm, 422.4 mm, and 846.8 mm separation cases. A more detailed view of the pressure ratio along the longitudinal axes outside the nozzles is presented in Figure 21. The velocity along the longitudinal axes of the nozzles is presented in a similar manner in Figure 22.

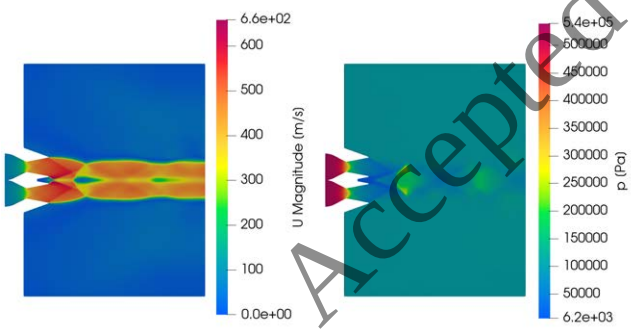

Figure 12 Distance: 70.4 mm.

It can be observed that in all cases, the pressure at the nozzle exit (where $X/X_g = 2$) is lower than atmospheric pressure, indicating that the nozzles are over-expanded. As a result, the external pressure causes the flows to converge and move vertically away from the longitudinal axes of the nozzles.

Regarding the interaction between the nozzles, the first case, which has the smallest separation, shows a notable modification of the pressure ratio and velocity along the longitudinal axis due to the proximity of the nozzles. As the nozzles are separated further, the pressure distribution approaches that of a single nozzle, as illustrated in the seventh case, which corresponds to

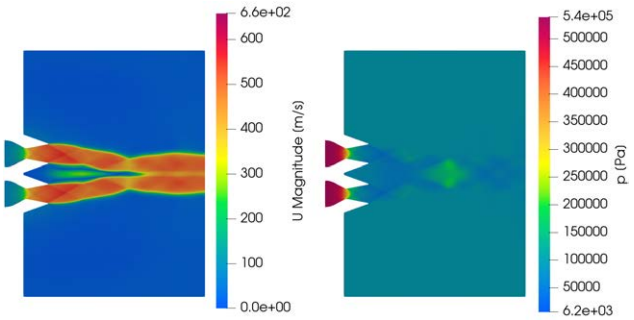

Figure 13 Distance: 105.6 mm.

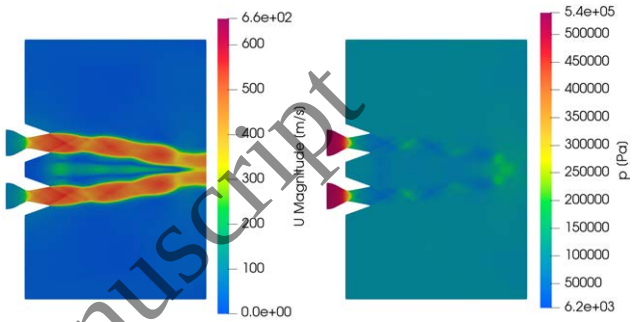

Figure 14 Distance: 140.8 mm.

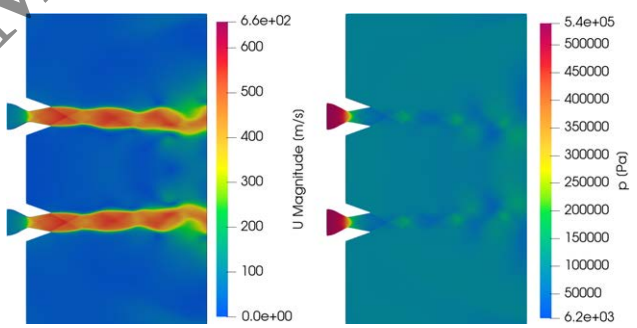

Figure 15 Distance: 281.6 mm.

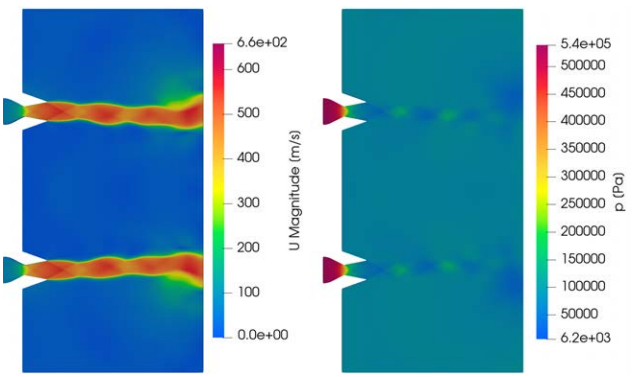

Figure 16 Distance: 422.4 mm.

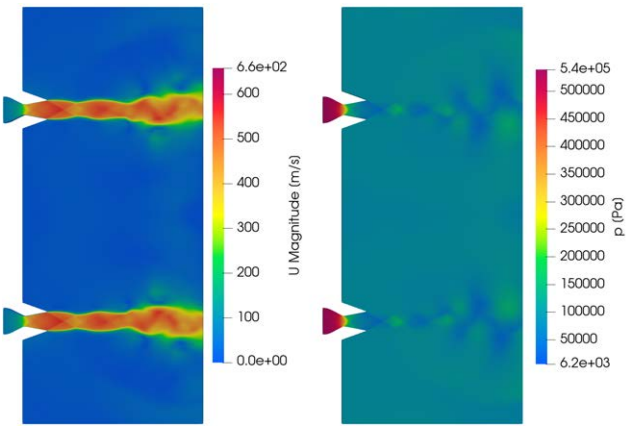

Figure 17 Distance: 563.2 mm.

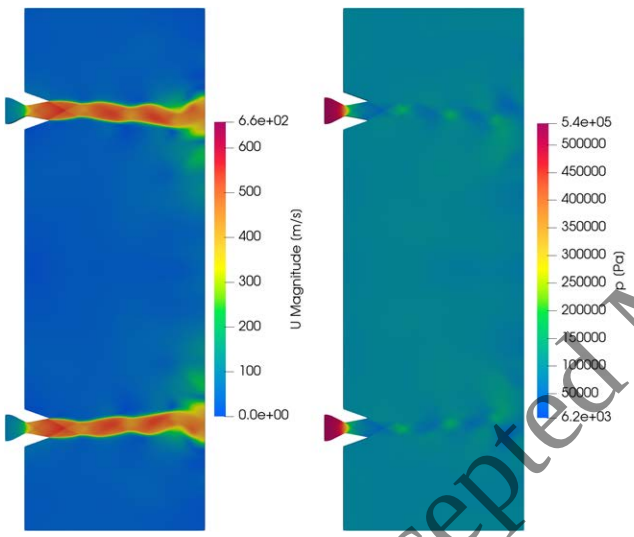

Figure 18 Distance: 846.8 mm.

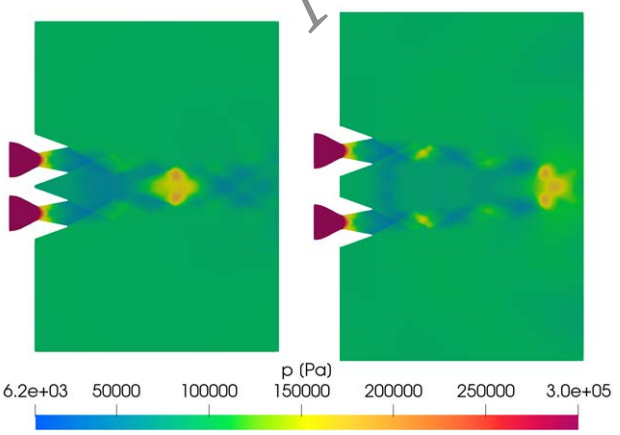

Figure 19 Left: 105.6 mm separation. Right: 140.8 mm separation.

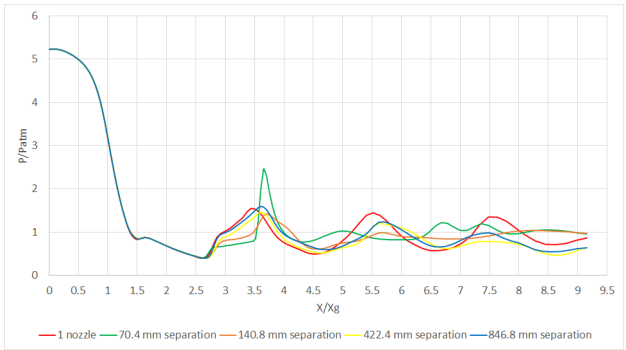

Figure 20 Pressure curves at the nozzles longitudinal axes.

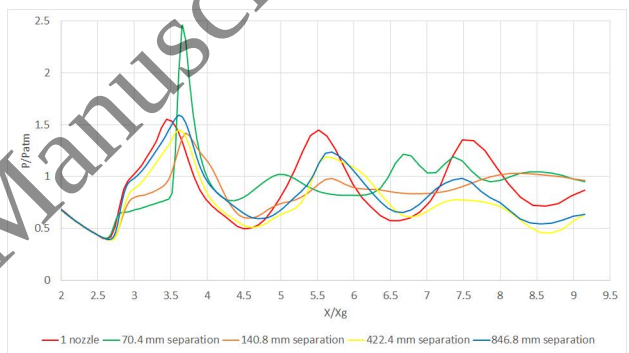

Figure 21 Pressure curves at the longitudinal axes outside the nozzles.

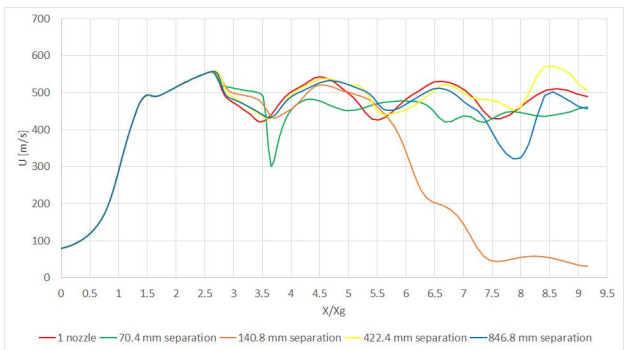

Figure 22 Velocity curves at the nozzles longitudinal axes.

a separation of 846.8 mm.

The third case, with a separation of 140.8 mm, is particularly interesting. In this scenario, the distance between the nozzles allows the discharge flows to close off relatively quickly. Consequently, the pressure distribution along the longitudinal axes of each nozzle nears atmospheric pressure and the velocity decreases rapidly shortly after exiting the nozzles.

Notably, the results inside the nozzles remain consistent across all simulations. This consistency is attributed to the exit flow being supersonic; any disturbance created by the second nozzle cannot travel upstream into the first nozzle.

Finally, it is emphasized that the discharge flow of each nozzle is influenced by the flow from the other nozzle. This interaction decreases when the separation between nozzle axes exceeds 8 or 9 times the radius of the exit section, although it does not completely disappear.

5. Conclusions

The numerical interaction of exit flows from two parallel Laval nozzles was examined using the OpenFOAM platform, assuming inviscid flow. The aim was to determine how the discharge from one nozzle influences the other.

As for the simulation results, it can be said that the validation studies for one nozzle yielded similar results to experimental studies and previous simulations.

Regarding the parallel nozzles, the pressure distribution inside each nozzle was not influenced by the presence of the second nozzle, as expected due to the supersonic nature of the flow. However, outside the nozzles, significant modifications to the discharge flow were observed, even in the case with the largest separation of 845.8 mm. It was noted that, because the flows were over-expanded, they tended to converge towards each other, moving away from the longitudinal axes of the nozzles.

Although our simulations involve simplifications, the results obtained are clear, indicating that interferences exist and must be considered in the design of rocket propulsion systems.

It is important to note that the open-source code OpenFOAM, specifically the *rhoCentralFoam* solver, has proven to be an effective tool for conducting non-viscous simulations.

Future research should use denser meshes and consider the effects of viscosity and turbulence to obtain more accurate and realistic results. Additionally, exploring larger distances between the nozzle axes may help identify the necessary separation to eliminate interference between the discharge flows. Furthermore, developing 3D simulations would enhance the study initiated here.

6. Declaration of competing interest

We declare that we have no significant competing interests, including financial or non-financial, professional, or personal interests interfering with the full and objective presentation of the work described in this manuscript.

7. Funding

This research was funded by Proyecto Consolidar, SECyT-Universidad Nacional de Córdoba: “Desarrollo y aplicación de estudios teóricos, numéricos y códigos computacionales en mecánica de fluidos e intermitencia caótica”.

8. Author contributions

Z.M. and S.E. conceived and designed the analysis. Z.M. collected the data. Z.M. and F.P. contributed data or analysis tools. Z.M., F.P. and S.E. performed the analysis. F.P. and S.E. wrote the paper.

9. Data availability statement

The authors confirm that the data supporting the findings of this study are available within the article.

References

[1] M. Ishibashi and M. Takamoto, “Very accurate analytical calculation of the discharge coefficient of critical venturi nozzles with laminar boundary layer,” in *Proceedings of International Symposium on Fluid Control, Measurement and Visualization (FLUCOME)*, Hayama, Japan, Sep. 1997.

[2] ——, “Discharge coefficient of super-accurate critical nozzle at pressurized condition,” in *Proceedings of the 4th International Symposium of Fluid Flow Measurement*, Denver, USA, Jun. 1999.

[3] H. Dietrich, E. Nath, and E. von Lavante, “High accuracy test rig for gas flows from 0.01 m^3/h up to 25000 m^3/h,” in *Proceedings of the International Measurement Confederation (IMEKO-XV) Congress*, Osaka, Japan, Jun. 1999.

[4] S. Som, A. Ramirez, L. D., and S. Aggarwal, “Effect of nozzle orifice geometry on spray, combustion, and emission characteristics under diesel engine conditions,” *Fuel*, vol. 90, pp. 1267–1276, 2011.

[5] R. Payri, F. Salvador, J. Gimeno, and J. de la Morena, “Effects of nozzle geometry on direct injection diesel engine combustion process,” *Applied Thermal Engineering*, vol. 29, pp. 2051–2060, 2009.

[6] S. Zarate-Orrego, G. Torres-Casierra, and E. del Risco-Moreno, "Horizontal vortex single chamber hydroturbine," *Revista Facultad de Ingeniería, Universidad de Antioquia*, vol. 79, pp. 150–162, 2016.
[7] A. Palencia-Diaz1, C. Barraza-Botet, and A. Bula-Silvera, "Experimental study of flat plate cooling using draft induced by a submerged radial jet," *Revista Facultad de Ingeniería, Universidad de Antioquia*, vol. 83, pp. 57–64, 2017.
[8] E. Love, D. Grigsby, L. Lee, and M. Woodling, "Experimental and theoretical studies of axisymmetric free jets," NASA, Technical Report TR R-6, 1959.
[9] N. Menon and B. Skews, "Effect of nozzle inlet geometry on underexpanded supersonic jet characteristics," in *Proceedings of 26th International Symposium of Shock Waves*, Germany, Jul. 2007.
[10] K. Hatanaka and T. Saito, "Influence of nozzle geometry on underexpanded axisymmetric free jet characteristics," *Shok Waves*, vol. 22, pp. 427–434, 2012.
[11] H. Kbab, T. Hamitouche, and Y. Mouloudj, "Study and simulation of the thrust vectoring in supersonic nozzles," *Journal of Advanced Research in Fluid Mechanics and Thermal Sciences*, vol. 93, pp. 13–24, 2022.
[12] C. Hunter, "Experimental, theoretical, and computational investigation of separated nozzle flows," *American Institute of Aeronautics and Astronautics*, no. 98-3107, 1998.
[13] Q. Xiao and M. Tsai, "Numerical investigation of supersonic nozzle flow separation," *AIAA Journal*, vol. 45, no. 3, 2007.
[14] OpenFOAM, *The OpenFOAM Foundation, "OpenFOAM v10 User Guide*.
[15] L. Gutierrez, J. Tamagno, and S. Elaskar, "An openfoam solver for high speed chemically active flows. simulation of planar detonations," *Computer Physics Communications*, vol. 219, pp. 209–222, 2017.
[16] L. Monaldi, G. Matallana, L. Gutierrez, and S. Elaskar, "Trayectoria del punto triple de una reflexión de onda de choque inestacionaria sobre pared recta," *Revista Facultad de Ciencias Básicas*, vol. 18, no. 2, pp. 63–70, 2022.
[17] L. Gutierrez, J. Tamagno, and S. Elaskar, "Numerical simulation of detonation cellular structures in h2-o2-ar mixtures with openfoam," *International Journal of Hydrogen Energy*, vol. 42, pp. 26 102–26 113, 2017.
[18] L. Gutierrez, S. Elaskar, J. Tamagno, J. Saldía, and G. Krause, "An assessment of the openfoam implementation of the knp scheme to simulate strong explosions," *Shock Waves*, vol. 31, pp. 193–202, 2021.
[19] L. Gutierrez, J. Tamagno, and S. Elaskar, "Numerical study on the impact of chemical modeling on simulating methane-air detonations," *Fuel*, vol. 240, pp. 289–298, 2019.
[20] J. Tamagno, W. Shulz, and S. Elaskar, *Dinámica de los gases, Flujo unidimensional estacionario*. Editorial Universitas, 2008.
[21] J. Blazek, *Computational Fluid Dynamics: Principles and Aplications*. Elsevier Ltd., 2005.
[22] L. Gutierrez, J. Tamagno, and S. Elaskar, "On building a rans, les or des energy equation for turbulent reacting flows," *Revista Facultad de Ingeniería, Universidad de Antioquía*, vol. 107, pp. 131–140, 2023.
[23] C. Geuzaine and J. Remacle, "Gmsh: a three-dimensional finite element mesh generator with built in pre- and post-processing facilities," *International Journal for Numerical Methods in Engi neering*, vol. 79, pp. 1309–1331, 2009.
[24] S. Bertolo and S. Elaskar, "Simulación numérica de del flujo compresible en toberas convergente-divergente," *Mecánica Computacional*, vol. 38, pp. 73–82, 2021.